EXPERIMENTAL STUDY OF THE NUCLEAR SPATIAL STRUCTURE OF NEUTRON-RICH He AND Li ISOTOPES

G.D. Alkhazov, A.V. Dobrovolsky, A.V. Khanzadeev, G.A. Korolev, A.A. Lobodenko, D.M. Seliverstov, A.A. Vorobyov

1. Introduction

To understand the evolution of sizes and shapes of nuclei in the nuclear chart from the valley of β-stability to the drip-line is one of the central questions of modern nuclear structure physics. Recent technique with radioactive beams has made it possible to reach the limit of the neutron drip-line for relatively light nuclei. Experimental studies have led to a discovery of significant neutron halos (skins) in these neutron-rich exotic nuclei. In nuclei near the drip-line, the separation energy of the last nucleon(s) becomes small. The valence nucleons of such loosely bound nuclei may have a very extended density distribution, called "halo". The necessary conditions for the halo formation have been intensively discussed. It was concluded that the nuclear states with small binding energy and low angular moment may form halos. The halo structure manifests itself in different types of reactions, in particular, by a large interaction cross section and by narrow momentum distributions of the reaction products in the processes of nuclear breakup and Coulomb dissociation. Note that the term "neutron skin" is used to describe an excess of neutrons over protons at the nuclear surface. It should be admitted however that a uniquely strict definition of the terms "skin" and "halo" does not exist. Some nuclei, such as ^{6}He and ^{8}He, are often referred to as neutron-skin as well as neutron-halo nuclei.

Experimental methods applied for studying halo nuclei were mainly measurements of the total interaction cross sections and investigations of momentum distributions of the reaction products after fragmentation. The spatial structure of exotic nuclei was proposed at PNPI to be studied by small-angle proton elastic scattering on nuclei. The proton-nucleus elastic scattering at intermediate energy is known to be an efficient means for studying the matter distributions in stable nuclei. This method can also be used in the inverse kinematics to study unstable short-lived nuclei. An advantage of proton scattering experiments at intermediate energy as compared to similar experiments at low energy is that at intermediate energy there exists a rather accurate multiple scattering theory of Glauber, which can relate the measured cross sections with the studied density distributions in quite an unambiguous way. The scattering of protons from the nuclear halo is confined to small scattering angles. Therefore, in order to study the spatial structure of halo nuclei it is important to measure with high accuracy the differential cross sections for proton scattering at small momentum transfers. The recoil detector IKAR, developed and built at PNPI [1], was adapted as an active hydrogen target in combination with a spectrometer for measurement of projectile scattering angles. Previously, IKAR was successfully used for investigation of small-angle hadron elastic scattering.

In experiments performed at GSI (Darmstadt) by the PNPI-GSI Collaboration, precise data on absolute differential cross sections for proton elastic scattering on stable ^{4}He, ^{6}Li and neutron-rich ^{6}He, ^{8}He, ^{8}Li, ^{9}Li, and ^{11}Li nuclei have been obtained in the inverse kinematics at an energy of about 0.7 GeV/nucleon at near-forward angles [2–4].

The matter radii and the radial structure of nuclear matter were derived from the data using the Glauber multiple scattering theory. Combining these results with results of other experiments permits one to obtain more details on the nuclear spatial structure.

2. Experimental setup and procedure

For the experiments, primary ^{18}O beams were extracted from the heavy-ion synchrotron SIS and focused on an 8 g/cm^2 beryllium production target at the entrance of the fragment separator FRS. Isotopes of helium and lithium nuclei produced by fragmentation of ^{18}O entered the FRS and were separated according to their magnetic rigidity. In some cases the separation power of the FRS was enhanced by inserting an achromatic (20 g/cm^2) aluminum degrader at the dispersive central focal plane for achieving isotopically pure beams. Beam intensities were generally 10^3 s^{-1} with the duty factor between 25% and 50%.

The arrangement of detectors for the scattering experiment is shown in Fig. 1. The main constituent of the setup was the hydrogen-filled ionization chamber IKAR at a pressure of 10 bar, which served simultaneously as a gas target and a recoil proton detector. The recoil protons were registered in IKAR in coincidence with the scattering projectiles. The momentum transfer could be determined either from the measured energy of the recoil protons or from the value of the scattering angle Θ_s of the projectiles which was measured by a tracking detector consisting of 2 pairs of two-dimensional multiwire proportional chambers (PC1-PC2 and PC3-PC4), arranged upstream and downstream with respect to IKAR. A set of scintillation counters (S1, S2 and S3) were used for triggering and identification of the beam particles *via* time-of-flight and *dE/dx* measurements, and a circular-aperture scintillator VETO was used to select projectiles that entered IKAR within an area of 2 cm in diameter around the central axis. In the experiment with the secondary beams of the lithium isotopes, the experimental setup was supplemented with a magnetic-rigidity analysis of the scattered particles (with the help of a dedicated dipole magnet ALADIN and a scintillator wall behind it) for the reliable separation of the projectile break-up channels. The quality of the isotope separation achieved is demonstrated in Fig. 2 for the case of the ^{11}Li scattered beam, where the ejectile horizontal plane X-coordinate measured at the scintillator wall is plotted *vs* the horizontal plane scattering angle Θ_x for the Li isotopes, these measurements being performed in coincidence with the IKAR signals corresponding to scattering events. It is seen that the projectile breakup channels could easily be discriminated.

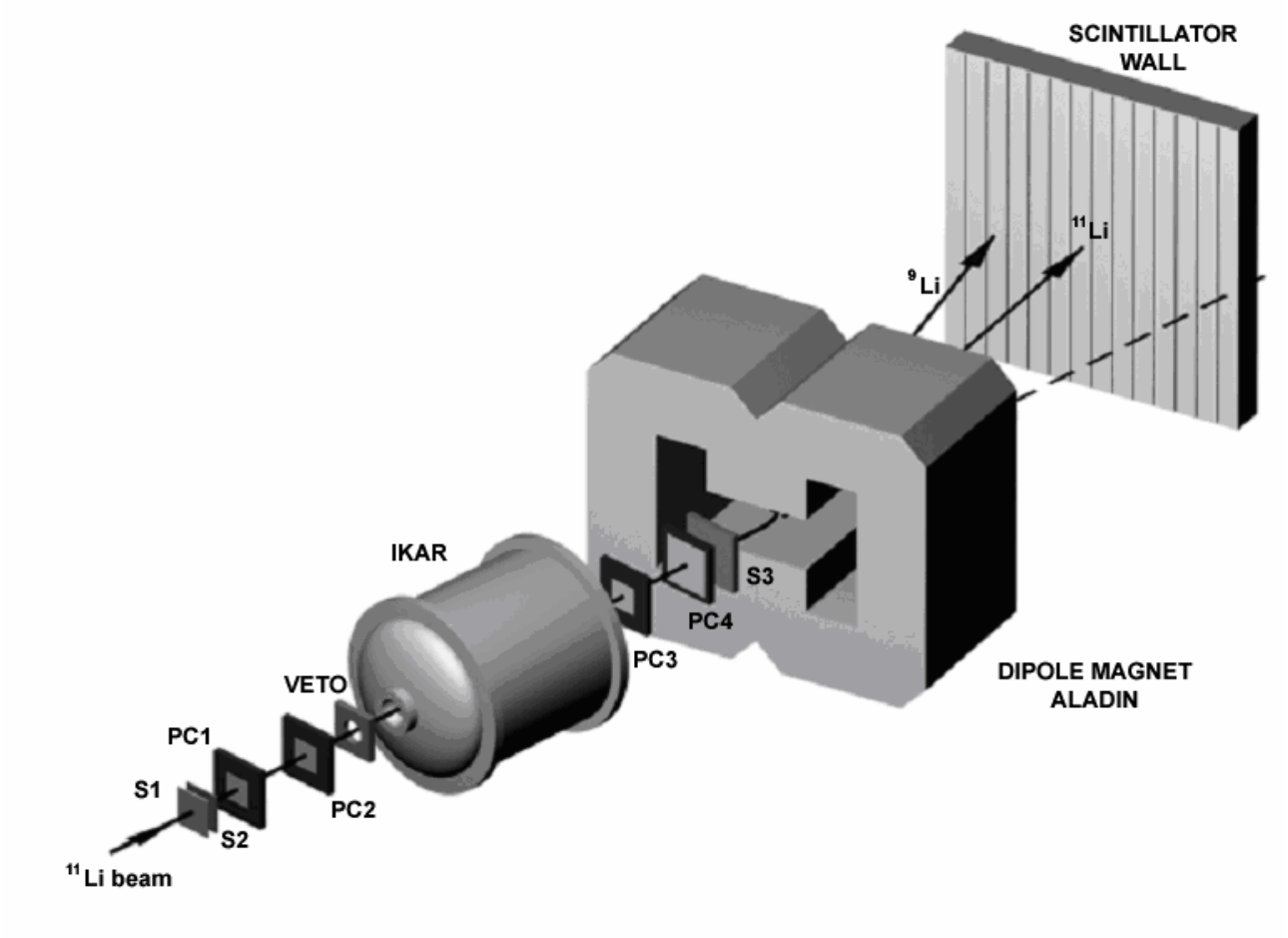

Fig. 1. Schematic view of the experimental setup for small-angle proton elastic scattering on exotic nuclei in the inverse kinematics. The central part shows the hydrogen-filled ionization chamber IKAR, which serves simultaneously as gas target and detector system for recoil protons. In six independent sections of this detector the recoil energy T_R, the recoil angle Θ_R and the vertex point Z_v are determined. The forward spectrometer consisting of four multi-wire proportional chambers PC1–PC4 determines the scattering angle Θ_S of the projectile. The scintillation counters S1–S3 and VETO are used for beam identification and triggering. The dipole magnet ALADIN with a position-sensitive scintillator wall behind allows to identify the scattered beam particle and to discriminate breakup channels

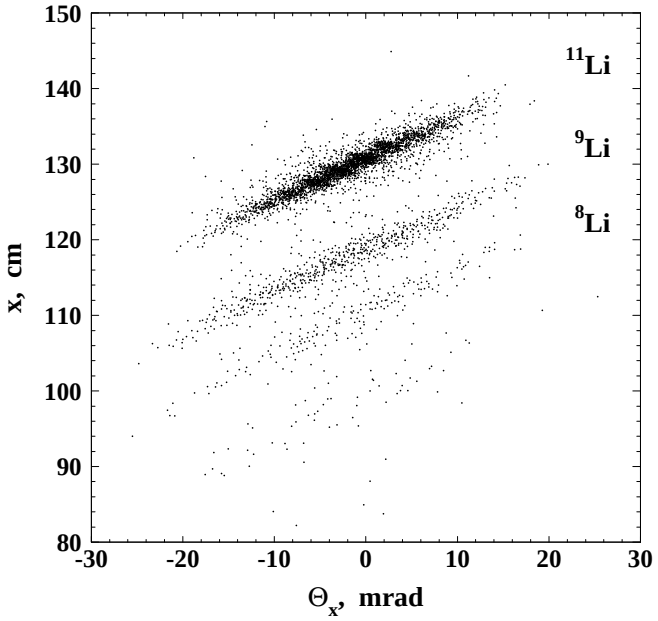

Fig. 2. Correlation between the measured ejectile horizontal X-coordinate behind the ALADIN magnet and the scattering angle Θ_x for the case of the ^{11}Li beam

The absolute differential cross section $d\sigma/dt$ is determined from the relation

$$\frac{d\sigma}{dt} = \frac{dN}{dt \cdot Mn \cdot \Delta L} \ . \qquad (1)$$

Here, dN is the event rate of elastic pHe or pLi scattering in the interval dt of the four-momentum transfer squared, and M is the corresponding rate of beam particles hitting the target. The quantity n is the density of the target nuclei known from the measured H_2 gas pressure and temperature, and ΔL denotes the effective target length. The differential cross section for proton scattering at the energy of E_p= 0.7 GeV from the ^{4,6,8}He and ^{6,8,9,11}Li nuclei were measured in the t-range of 0.002 $(\text{GeV/c})^2 \le |t| \le 0.05$ $(\text{GeV/c})^2$ (Fig. 3). The systematic error of the cross section normalization was ~3%, while the uncertainty in the t-scale calibration was about 1.5%.

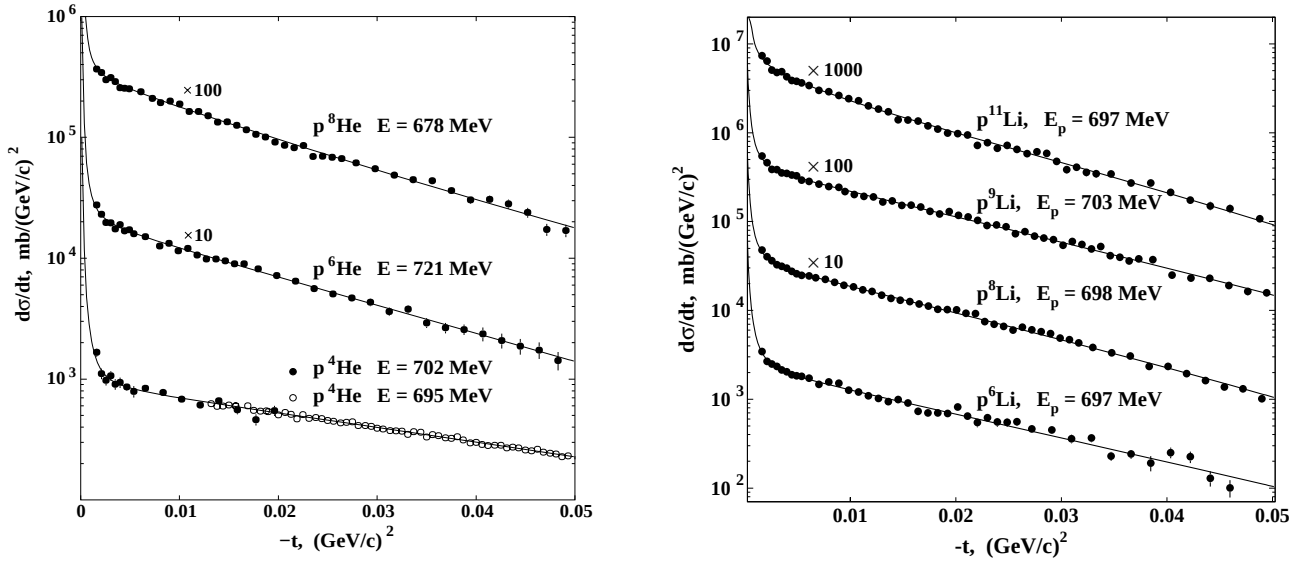

Fig. 3. Absolute differential cross sections $d\sigma/dt$ *vs* the four momentum transfer squared t for p^4He, p^6He, and p^8He (left side), and p^6Li, p^9Li, and p^{11}Li (right side) elastic scattering measured in the present experiment (full dots). For p^4He scattering, the open dots show the data of Ref. [5]. Plotted lines are obtained by calculations using the Glauber multiple scattering theory

The measurement of $d\sigma/dt$ for p^4He scattering was carried out for the main purpose of providing a reference to the known precise data of the IKAR experiment [5] performed in the direct kinematics. Good agreement between both sets of data (see Fig. 3) gives confidence to the novel experimental approach applied in this work.

For establishing the nuclear density distributions from the measured cross sections, the Glauber multiple scattering theory was applied. Calculations were performed using the basic Glauber formalism for proton-nucleus elastic scattering and taking experimental data on the elementary proton-proton and proton-neutron scattering amplitudes as input. In the analysis, four parameterizations for phenomenological nuclear density distributions have been applied, labeled as SF (symmetrized Fermi), GH (Gaussian-halo), GG (Gaussian-Gaussian) and GO (Gaussian-oscillator). Each of these parameterizations has two free parameters. While the SF and GH parameterizations do not make any difference between the neutron and proton distributions, the GG and GO parameterizations assume that the nuclei consist of core nucleons and valence nucleons with different spatial distributions. The core distribution is assumed to be a Gaussian one in both the GG and GO parameterizations. The valence nucleon density is described by a Gaussian or a 1p shell harmonic oscillator-type distribution within the GG or GO parameterizations, respectively. The free parameters in the GG and GO parameterizations are the r.m.s. radii R_c and R_v of the core and valence nucleon distributions. It was assumed that the considered nuclei have one (^{8}Li), two (^{6}He, ^{6}Li, ^{9}Li, ^{11}Li) or four (^{8}He) valence nucleons. The free parameters of the model density distributions have been deduced by fitting the calculated cross sections to the experimental ones in the t-range covered by the experiment. For p^4He scattering, the data of this experiment and those of Ref. [5], measured in a wider t-interval, were analyzed together.

3. Results on the matter density distribution and radii

The solid curves in Fig. 3 represent the results of the calculations performed using phenomenological density distributions with fitted parameters. At very small values of $|t|$, the steep rise of the cross sections with $|t|$ decreasing is due to the Coulomb scattering. As for the cross sections at larger values of $|t|$ (at $|t| > 0.005$ (GeV/c)^2 where the contribution from the Coulomb scattering is small), at first glance the measured cross sections plotted in the logarithmic scale look like straight lines, that is the cross sections seem to have an exponential t-dependence. However, at closer examination it is possible to see that the t-dependence of the cross sections at 0.005 (GeV/c)$^2 < |t| < 0.05$ (GeV/c)^2 in the cases of p^4He and $p^{8,9}$Li scattering is indeed very close to the exponential one, whereas the shape of the cross sections in the cases of $p^{6,8}$He and $p^{6,11}$Li scattering deviates noticeably from the exponential form. This deviation can be seen if one plots the cross sections divided by exponential functions. Such a plot is presented in Fig. 4. It is seen that the p^{11}Li, p^6He, p^8He and p^6Li cross sections are not consistent with the exponential form, that can be explained by the fact that the contributions to the cross section of proton scattering from the core and from the halo of these nuclei have different angular dependences, the contribution of scattering from the halo decreasing with $|t|$ increase faster than that from the core. The fact that halo nuclei demonstrate positive curvature in log ($d\sigma/dt$) was supported by simulation calculations [2, 4] for the cases of ^{6}He and ^{11}Li.

The parameterizations SF and GH applied for ^{4}He allowed us to describe the data equally well and have yielded identical values of the matter radius. The experimental differential cross sections for the case of ^{6}He, ^{6}Li, ^{8}He, ^{8}Li, and ^{9}Li are well described with the four density parameterizations used, the reduced value of χ^2 being around unity. For these nuclei, the matter density distributions obtained with the GG and GO parameterizations are very similar to those obtained with the SF and GH parameterizations, the deduced r.m.s. matter radii being practically the same for the four versions of the analysis. All versions of the analysis also resemble each other in reproducing extended matter distributions in ^{6}He and ^{8}He, the matter density decreasing with the radial distance r increase much slower than that for ^{4}He.

A simple geometrical classification scheme has been suggested by theorists, where the ratio of the valence nucleon to core nucleon radii $\kappa = R_v/R_c$ is used as a gauge for the halo. For light neutron-rich nuclei close to the valley of β-stability theory predicts typically $\kappa \sim 1.20$–1.25, while for halo nuclei this values can be essentially larger, up to $\kappa \geq 2$. Fig. 5 shows for the case of p^{11}Li scattering the value of χ^2, which serves as a quantitative criterion for the quality of the theoretical description of experimental data, the fitted cross sections being

calculated with different values of the assumed ratio R_h/R_c of the halo (R_h) and core (R_c) r.m.s. radii. It is seen that good data description is achieved only in the case when the halo radius is significantly larger than that of the core, the fitted value of R_h/R_c being 2.46 (17). This figure demonstrates high sensitivity of the proton scattering cross sections at small momentum transfers to the halo structure of exotic nuclei.

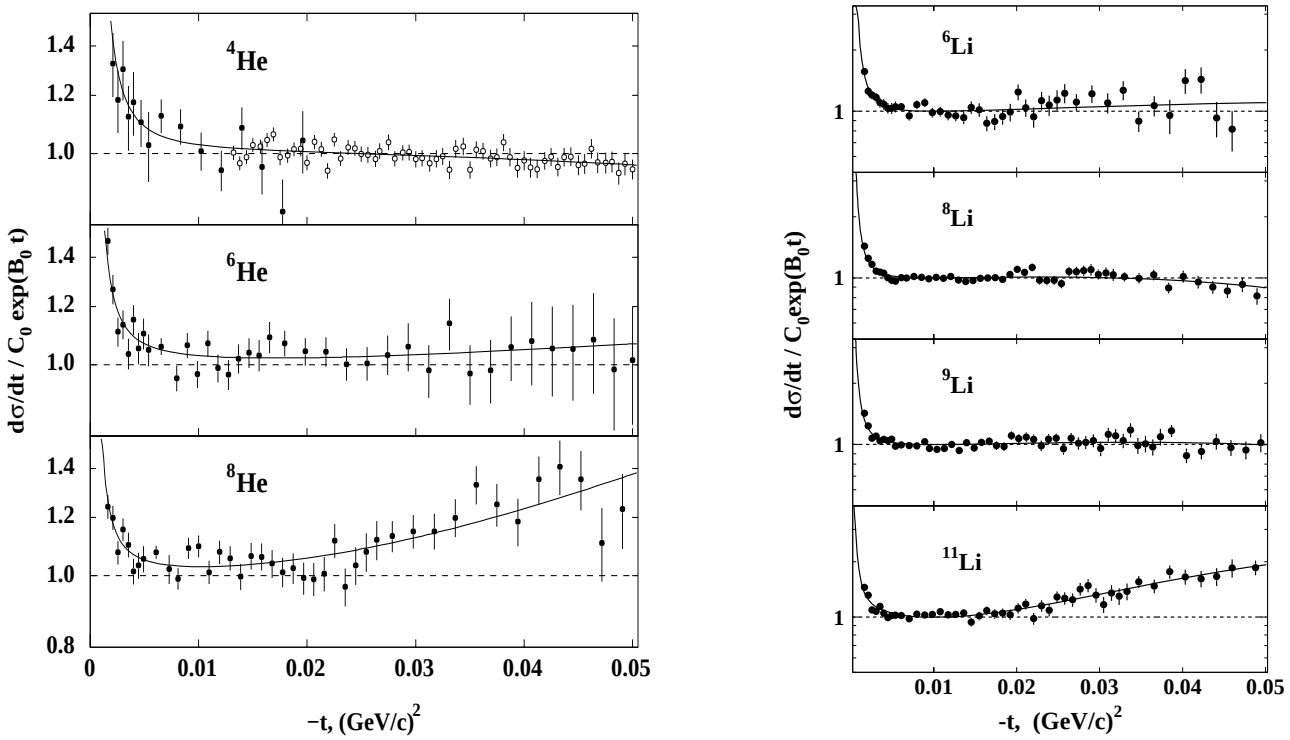

Fig. 4. Measured differential cross sections for He and Li isotopes divided by an exponent. The positive curvature in $\log(d\sigma/dt)$ is a fingerprint of isotopes with an extended density distribution. The ^{11}Li nucleus with the largest halo shows the most pronounced positive curvature

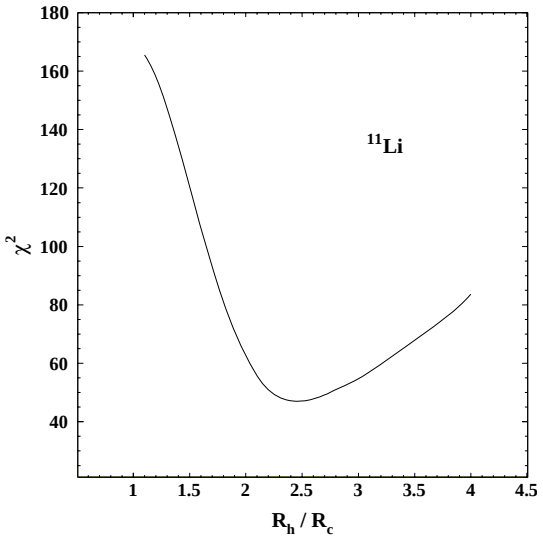

Fig. 5. The value of χ^2, serving as quantitative criterion for the quality of p^{11}Li differential cross section description, as a function of the assumed ratio R_h/R_c of the halo and core radii of ^{11}Li.

It should be noted that the data on small-angle proton scattering have low sensitivity to a possible contribution of long halo density tails, which are predicted by theory for nuclei with low binding energy. Taking such tails from theory may increase the deduced radii by 0.1–0.2 fm in the case of ^{6}He and ^{8}He [2] and by ~0.3 fm in the case of ^{11}Li [4].

The results obtained for helium and lithium isotopes in this experiment are presented in Table 1. This table presents the r.m.s. radii R_m, R_c, and R_v of the matter, core and valence nucleon distributions, and the ratio $\kappa = R_v/R_c$ deduced from the data. It is seen that the matter radii of the ^{6}He, ^{8}He and ^{11}Li nuclei are significantly larger that those of the lighter He and Li isotopes. In the case of ^{4}He and ^{6}Li, which are the $N = Z$ nuclei, the matter density distributions and radii determined from the data on proton scattering are in good agreement with the proton distributions deduced from the known data on electron scattering. The ^{8}Li and ^{9}Li nuclei do not have noticeable signatures of the halo-like structure. However ^{6}He, ^{8}He and ^{11}Li exhibit a halo-like structure, the ^{11}Li nucleus having the most pronounced halo.

Table 1

Summary of the results obtained for helium and lithium isotopes in the present experiment. The values R_m, R_c and R_v denote the r.m.s. radii of the matter, core and valence nucleon(s) distributions, κ is the ratio R_v/R_c. As mentioned in the text, R_m (and R_v) for ^{6}He, ^{8}He and ^{11}Li are deduced taking into account long density tails predicted by theory at the nuclear far periphery

Nucleus	R_m, fm	R_c, fm	R_v, fm	$\kappa = R_v/R_c$
^{4}He	1.49 (3)	–	–	–
^{6}He	2.45 (10)	1.88 (12)	3.31 (28)	1.76
^{8}He	2.53 (8)	1.55 (15)	3.22 (14)	2.08
^{6}Li	2.44 (7)	2.11 (17)	3.00 (34)	1.42
^{8}Li	2.50 (6)	2.48 (7)	2.58 (48)	1.03
^{9}Li	2.44 (6)	2.20 (6)	3.12 (28)	1.41
^{11}Li	3.71 (20)	2.53 (3)	6.85 (58)	2.71

The matter distributions deduced for ^{8}Li and ^{9}Li turn out be quite similar to each other (Fig. 6). Within the quoted errors the matter radii of ^{8}Li and ^{9}Li are equal to that of ^{6}Li. This means that ^{8}Li and especially ^{9}Li are more dense nuclei than ^{6}Li, the latter being considered to have an $\alpha + d$ spatial structure.

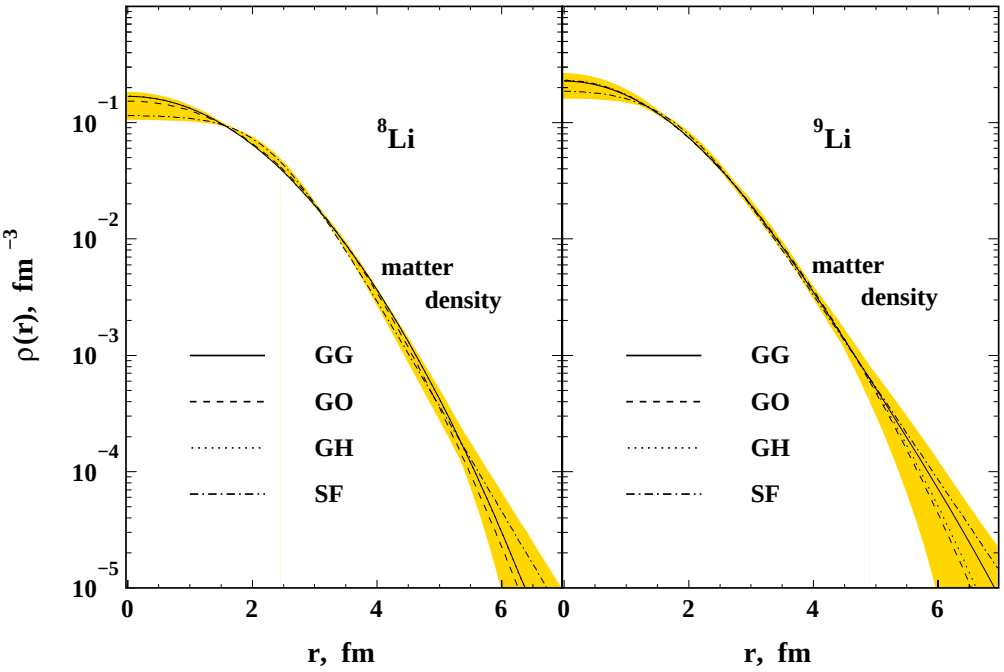

Fig. 6. Nuclear matter density distributions in ^{8}Li and ^{9}Li deduced from the present data. Solid, dashed, dotted and dash-dotted lines correspond to the densities obtained using the SF, GH, GG and GO density distribution parameterizations, respectively. The shaded areas represent the envelopes of the density variation within the model parameterizations applied, superimposed by the statistical errors. The nuclear density distributions are normalized to the total number of nucleons

Figure 7 shows the core and total matter density distributions derived for ^{11}Li and ^{8}He using phenomenological density distributions. It is seen that while in the case of ^{8}He it might be still questionable whether the valence neutron distribution should be called halo or skin, the observed extended valence neutron distribution in ^{11}Li at the nuclear far periphery is decidedly an outstanding neutron halo.

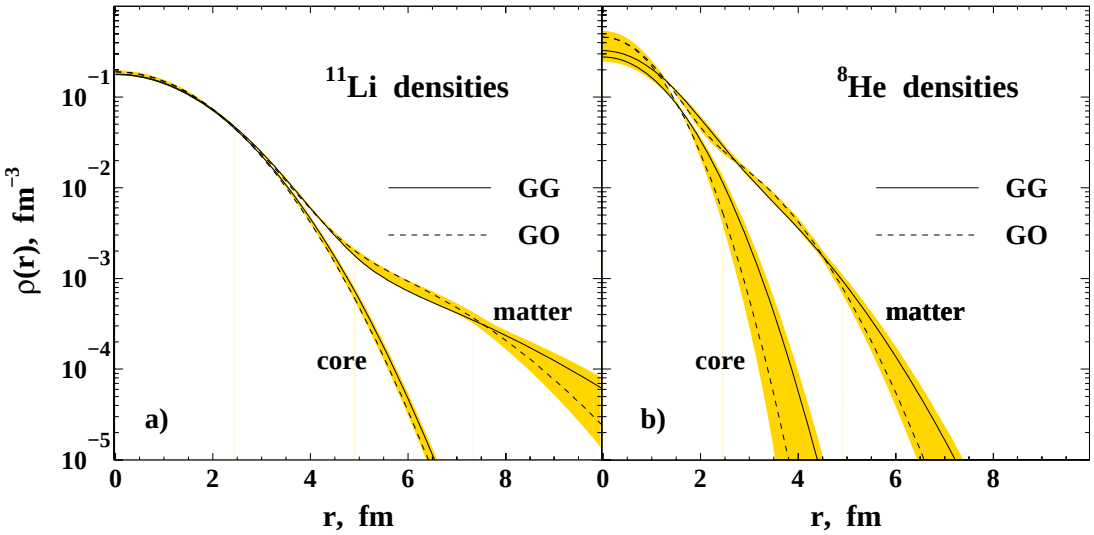

Fig. 7. (a) Nuclear core and total matter density distributions in ^{11}Li deduced from the present data using the GG and GO density distribution parameterizations. (b) Similar distributions in ^{8}He. The shaded areas represent the envelopes of the matter and core density variations within the model parameterizations applied, superimposed by the statistical errors

Recent precise measurements of the charge radii by the laser spectroscopy for ^{6}He and ^{8,9,11}Li permit to extract the r.m.s. radii R_p of proton distributions (see Table 2). Combining these values and the value of R_m deduced from the data on proton elastic scattering, it is easy to obtain the radii of the neutron distributions R_n of these nuclei. The thickness of the neutron skin $\delta_{np} = R_n - R_p$ can also be determined (Table 2).

In the experiment on the Coulomb dissociation of ^{6}He performed recently at GSI, new information on the structure of the ground state wave function was obtained. It was found that the mean square distance between the center-of-mass (CM) of the ^{6}He system and that of the α-particle core is $R_{\alpha}^{CM} = 1.12\ (13)$ fm, while the distance between the CM of the ^{6}He system and that of the two halo neutrons is $R_{2n}^{CM} = 2.24\ (26)$ fm. Combining these values with the radii from Table 2 it is possible to find for ^{6}He the radius of the proton distribution in the core center $R_p^* = [R_p^2 - (R_{\alpha}^{CM})^2]^{1/2} = 1.55\ (10)$ fm and the radius of the di-neutron cluster $R_{dn}^* = [R_h^2 - (R_{2n}^{CM})^2]^{1/2} = 2.45\ (48)$ fm. The determined size of the di-neutron cluster (or the distance between the two neutrons $R_{nn} = 2\,R_{dn}^*$) denotes a weak attractive correlation between the halo neutrons. It means that the di-neutron configuration of halo neutrons in ^{6}He predominates over cigar-like configuration [6].

Table 2

Neutron radii R_n and neutron skin thicknesses $\delta_{np} = R_n - R_p$, derived from matter radii R_m (present experiment) and proton radii R_p (laser spectroscopy experiments)

Nucleus	R_m, fm	R_p, fm	R_n, fm	δ_{np}, fm
^{6}He	2.45 (10)	1.91 (2)	2.68 (13)	0.77 (13)
^{8}Li	2.50 (6)	2.16 (3)	2.68 (9)	0.52 (10)
^{9}Li	2.44 (6)	2.09 (4)	2.60 (8)	0.51 (9)
^{11}Li	3.71 (20)	2.37 (4)	4.10 (25)	1.73 (25)

4. Conclusion

A new method to study the nuclear spatial structure of exotic nuclei by small-angle proton elastic scattering in the inverse kinematics has been proposed and developed at PNPI. The positive curvature in log $d\sigma/dt$ at small momentum transfers can be used as a qualitative indication of a possible halo existence. The method also permits to obtain from the data the matter, core and valence nucleon r.m.s. radii. The ratio of the valence nucleon to core nucleon radii gives a parameter for the quantitative measure for the halo structure.

Successful measurements of p^4He, p^6He, p^8He, p^6Li, p^8Li, p^9Li, and p^{11}Li elastic scattering were performed at an energy of 0.7 GeV/u at GSI, Darmstadt. Absolute differential cross sections were obtained with the experimental setup where the main constituent was an active target-recoil detector IKAR. The obtained results clearly demonstrate the halo structure of ^{6}He, ^{8}He and ^{11}Li, the most prominent halo being observed for ^{11}Li.

New measurements with the same experimental techniques were performed on B and Be ion beams at GSI in 2005 and 2006. Small-angle proton elastic scattering from the ^{7}Be, ^{9}Be, ^{10}Be, ^{11}Be, ^{12}Be, ^{14}Be and ^{8}B nuclei was studied. The most interesting among these nuclei are ^{8}B, for which the proton halo existence is expected, and ^{11}Be and ^{14}Be, for which significant neutron halos are expected. An analysis of the experimental data is in progress.

The data presented in this article have been measured and analyzed by the IKAR Collaboration:
G.D. Alkhazov, M.N. Andronenko, A.V. Dobrovolsky, G.E. Gavrilov, A.V. Khanzadeev, G.A. Korolev, A.A. Lobodenko, D.M. Seliverstov, N.A. Timofeev, A. A.Vorobyov, V.I .Yatsoura (PNPI, Gatchina), A. Baucher, P. Egelhof, S. Fritz, H. Geissel, C. Gross, H. Irnich, G. Kraus, G. Münzenberg, S. R .Neumaier, T. Schäfer, C. Scheidenberg, W. Schwab, T. Suzuki (GSI, Darmstadt), M. Mutterer (IKP TU, Darmstadt).

References

1. A.A. Vorobyov, G.A. Korolev, V.A. Schegelsky *et al*., Nucl. Instr. Meth. **119**, 509 (1974).
2. G.D. Alkhazov, A.V. Dobrovolsky, P. Egelhof *et al*., Nucl. Phys. A **712**, 269 (2002).
3. S.P. Neumaier, G.D. Alkhazov, M.N. Andronenko *et a*l., Nucl. Phys. A **712**, 246 (2002).
4. A.V. Dobrovolsky, G.D. Alkhazov, M.N. Andronenko *et al*., Nucl. Phys. A **766**, 1 (2006).
5. O.G. Grebenyuk, A.V. Khanzadeev, G.A. Korolev *et al*., Nucl. Phys. A **500**, 637 (1989).
6. G.D. Alkhazov, A.V. Dobrovolsky and A.A. Lobodenko, Yad. Fiz. **69**, 1157 (2006) [Phys. Atom. Nucl. **69**, 1124 (2006)].